Theoretical investigation of the Freeman resonance in the dissociative ionization of H$_2^+$

Jinzhen Zhu [*]

Physics Department, Ludwig Maximilians Universität, D-80333 Munich, Germany

The dissociative ionization of H$_2^+$ in linearly polarized, 400 nm laser pulses is simulated by solving a three-particle time-dependent Schrödinger equation in full dimensionality. The joint energy spectra (JES) are computed for cos^8 and flat-top envelopes using the time-dependent surface flux (tSurff) methods. In JES, the energy sharing of N photons with frequency ω by nuclear kinetic energy release (KER) E_N and electronic KER E_e is well described by $E_N + E_e = N\omega - U_p + E_0$ for the cos^8 envelope, but satisfy $E_N + E_e = N\omega + E_0$ for the flat-top envelope, exposing a deviation of the ponderomotive energy U_p, where E_0 is the ground energy of H$_2^+$ and this observation has been observed in experiments. The analysis of the wave function for electrons and protons after the pulse are presented, where we find U_p is absorbed by the Freeman resonances between two excited ungerade states of H$_2^+$.

I. INTRODUCTION

Being a typical candidate for the investigation of the three-body Coulomb interaction problem in attosecond physics, H$_2^+$ has been investigated a lot both on experimental and theoretical sides [1–14]. The JES of the KER for one electron E_e and two protons E_N of the H$_2^+$ ion are predominant observables that show how energy is distributed around the fragments.

As required by quantum mechanics and law of energy conservation, the equation $E_N + E_e = N\omega + E_0 - U_p$ for multiphoton ionization is preferred in JES, which means that the total energy of the three particles is N photons ω subtracted by the ponderomotive energy of the electron U_p. Wu *et al.* [13] reported the energy sharing of fragments of H$_2$ in the JES in experiments using 400 nm linearly polarized and long pulses. Their observations are also helpful for the investigation of H$_2^+$, because in experiments, H$_2^+$ are created from H$_2$. In their experiments $E_N + E_e$ lines do not move considerably for intensities 5.9×10^{13} and 4.3×10^{13} W/cm^2, which means the contribution of intensity dependent U_p is missing, because of Freeman resonances [15]. However, relative theoretical studies on a 400 nm computation have not been reported yet.

The difficulties for theoretical studies mainly comes from the computational cost that grows exponentially with the wavelength and intensities. The scaling problem can be relived by using the time-dependent surface flux method (tSurff) [16], which has been applied to another three-body system He in full dimensionality [17,18], and also has been successfully applied to two-dimensional (2D) models [9,10]. The dissociative ionization of the H$_2^+$ has also been simulated in reduced dimensionality by other groups [11,19–25], where the nuclear KER is most probable around 0.5 atomic units, far from experimental observations. Our previous paper [26] reported

the dissociative ionization of H$_2^+$ ion in full dimensionality and gives the nuclear KER (2–4 eV) close to experimental observables [12–14].

In this paper we will investigate the Freeman resonance of dissociative of H$_2^+$ by quantum simulations in full dimensionality based on the tRecX code.

II. COMPUTATIONAL DETAILS

In this paper, atomic units $\hbar = e^2 = m_e = 4\pi\epsilon_0 \equiv 1$ are used if not specified. Spherical coordinates with center of the mass of two protons as the origin are applied. Instead of using the vector between two protons $\vec{R}$ as a coordinate [9,10,22], we specify the coordinates of the protons and electrons as $\vec{r}_1$, $-\vec{r}_1$, and $\vec{r}_2$. We denote $M = 1836$ atomic units as the mass of the proton.

A. Hamiltonian

The wave function is depicted by $\psi(\vec{r}_1, \vec{r}_2, t)$ that satisfies $i\partial_t \psi(\vec{r}_1, \vec{r}_2, t) = H\psi(\vec{r}_1, \vec{r}_2, t)$. The total Hamiltonian can be represented by the sum of the electron-proton interaction H_{EP} and two tensor products, written as

$$H = H^{(+)} \otimes \mathbb{1} + \mathbb{1} \otimes H^{(-)} + H_{EP}, \tag{1}$$

where the tensor products are formed by the identity operator $\mathbb{1}$ multiplied by the Hamiltonian for two protons ($H^{(+)}$) or for the electron ($H^{(-)}$). With the coordinate transformation used in Ref. [27], the single operator for the electron is

$$H^{(-)} = -\frac{\Delta}{2m} - i\beta\vec{A}(t) \cdot \vec{\nabla}, \tag{2}$$

and the Hamiltonian for protons can be written as

$$H^{(+)} = -\frac{\Delta}{4M} + \frac{1}{2r}, \tag{3}$$
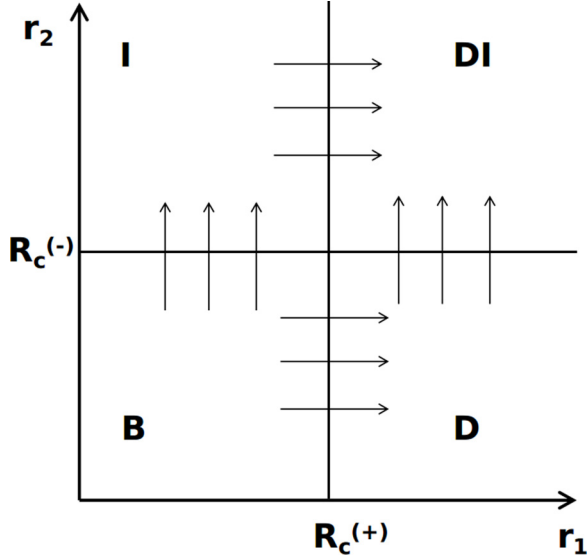
---

[*]Jinzhen.Zhu@physik.uni-muenchen.de

FIG. 1. The regions of dissociative ionization time propagation. The B stands for bound region, D for dissociation region where the two protons are out of $R_c^{(+)}$ but the electron is not ionized and stays inside. I represents the ionization region where the electron is out-of-box $R_c^{(-)}$ but the two protons are still inside $R_c^{(+)}$. DI stands for the dissociative ionization region where both the electron and the protons are out of $R_c^{(+/-)}$. $R_c^{(+/-)}$ are the tSurff radii for $r_1 = |\vec{r}_1|$ or $r_2 = |\vec{r}_2|$.

where we introduce reduced mass $m = \frac{2M}{2M+1} \approx 1$ and $\beta = \frac{1+M}{M} \approx 1$ for the electron. The Hamiltonian of the electron-proton interaction can be written as

$$H_{EP} = -\frac{1}{|\vec{r}_1 + \vec{r}_2|} - \frac{1}{|\vec{r}_1 - \vec{r}_2|}. \quad (4)$$

B. Computational methods

The tSurff method is applied for computing the JES and is detailed in our previous works [17,26]. A simplified version with important points is presented here for completion.

Following the essence of the tSurff method, we neglect the interactions of protons and electrons beyond a sufficient large tSurff radius $R_c^{(+/-)}$, with the corresponding Hamiltonians being $H_V^{(+)} = -\frac{\Delta}{4M}$ for two protons and $H_V^{(-)} = -\frac{\Delta}{2m} - i\beta\vec{A}(t) \cdot \vec{\nabla}$ for the electron. The scattered states of the two protons and the electron are Volkov solutions, which satisfy $i\partial_t \chi_{\vec{k}_1}(\vec{r}_1) = H_V^{(+)} \chi_{\vec{k}_1}(\vec{r}_1)$ and $i\partial_t \chi_{\vec{k}_2}(\vec{r}_2) = H_V^{(-)} \chi_{\vec{k}_2}(\vec{r}_2)$, respectively, where $\vec{k}_{1/2}$ denote the momenta of the protons or the electron.

Based on the tSurff radius $R_c^{(+/-)}$, we may split the dissociative ionization into four regions, namely B, I, D, DI, shown in Fig. 1, where bound region B preserves the full Hamiltonian in Eq. (1), D, I are time propagations by single particles with the Hamiltonians being

$$H_D(\vec{r}_2, t) = H_V^{(-)}(\vec{r}_2, t) = -\frac{\Delta}{2m} - i\beta\vec{A}(t) \cdot \vec{\nabla} \quad (5)$$

and

$$H_I(\vec{r}_1, t) = -\frac{\Delta}{4M} + \frac{1}{2r_1}, \quad (6)$$

and DI is an integration process. The treatment was first introduced in the double ionization of helium in Ref. [28] and then applied in a 2D simulation of the H_2^+ ion in Ref. [9].

We assume that for a sufficiently long propagation time T, the scattering ansatz of the electron and protons disentangle. By introducing the step function

$$\Theta_{1/2}(R_c) = \begin{cases} 0, & r_{1/2} < R_c^{(+/-)}, \\ 1, & r_{1/2} \geqslant R_c^{(+/-)}, \end{cases} \quad (7)$$

the unbound spectra can be written as

$$P(\vec{k}_1, \vec{k}_2) = |b(\vec{k}_1, \vec{k}_2, T)|^2, \quad (8)$$

where the scattering amplitudes $b(\vec{k}_1, \vec{k}_2, T)$ are

$$b(\vec{k}_1, \vec{k}_2, T) = \langle \chi_{\vec{k}_1} \otimes \chi_{\vec{k}_2} | \Theta_1(R_c)\Theta_2(R_c) | \psi(\vec{r}_1, \vec{r}_2, t) \rangle$$
$$= \int_{-\infty}^{T} [F(\vec{k}_1, \vec{k}_2, t) + \bar{F}(\vec{k}_1, \vec{k}_2, t)] dt, \quad (9)$$

with two sources being

$$F(\vec{k}_1, \vec{k}_2, t) = \langle \chi_{\vec{k}_2}(\vec{r}_2, t) | [H_V^{(-)}(\vec{r}_2, t), \Theta_2(R_c)] | \varphi_{\vec{k}_1}(\vec{r}_2, t) \rangle \quad (10)$$

and

$$\bar{F}(\vec{k}_1, \vec{k}_2, t) = \langle \chi_{\vec{k}_1}(\vec{r}_1, t) | [H_V^{(+)}(\vec{r}_1, t), \Theta_1(R_c)] | \varphi_{\vec{k}_2}(\vec{r}_1, t) \rangle. \quad (11)$$

The single particle wave functions $\varphi_{\vec{k}_1}(\vec{r}_2, t)$ and $\varphi_{\vec{k}_2}(\vec{r}_1, t)$ satisfy

$$i\frac{d}{dt}\varphi_{\vec{k}_1}(\vec{r}_2, t) = H_D(\vec{r}_2, t)\varphi_{\vec{k}_1}(\vec{r}_2, t) - C_{\vec{k}_1}(\vec{r}_2, t) \quad (12)$$

and

$$i\frac{d}{dt}\varphi_{\vec{k}_2}(\vec{r}_1, t) = H_I(\vec{r}_1, t)\varphi_{\vec{k}_2}(\vec{r}_1, t) - C_{\vec{k}_2}(\vec{r}_1, t). \quad (13)$$

The sources are the overlaps of the two-electron wave function and the Volkov solutions shown by

$$C_{\vec{k}_1}(\vec{r}_2, t) = \int d\vec{r}_1 \overline{\chi_{\vec{k}_1}(\vec{r}_1, t)} [H_V^{(+)}(\vec{r}_1, t), \Theta_1(R_c)] \psi(\vec{r}_1, \vec{r}_2, t) \quad (14)$$

and

$$C_{\vec{k}_2}(\vec{r}_1, t) = \int d\vec{r}_2 \overline{\chi_{\vec{k}_2}(\vec{r}_2, t)} [H_V^{(-)}(\vec{r}_2, t), \Theta_2(R_c)] \psi(\vec{r}_1, \vec{r}_2, t), \quad (15)$$

with initial values being 0, where $\overline{\cdots}$ means complex conjugate. The two tSurff radii could be set as equivalent $R_c^{(+)} = R_c^{(-)}$, because all Coulomb interactions are neglected when either the protons or electron is out of the tSurff radius. According to our previous researches, the spectrum computation is independent of the R_c if all Coulomb terms are removed and the wave function is propagated long enough after the pulse [17,26,28]. Apart from the tSurff method, the infinite-range exterior complex scaling (irECS) method is utilized as an absorber [29].

C. Laser pulses

The dipole field of a laser pulse with peak intensity $I = \mathcal{E}_0^2$ (atomic units, $\mathcal{E}_0$ is the peak electric field) and linear polarization in the z direction is defined as $\mathcal{E}_z(t) = \partial_t A_z(t)$ with vector potential

$$A_z(t) = \frac{\mathcal{E}_0}{\omega} a(t) \sin(\omega t + \phi_{\text{CEP}}), \tag{16}$$

where ϕ_{CEP} is the phase of the pulse. The pulses with wavelength $\lambda = 400$ nm are applied with peak intensities 8.3×10^{13} and 5.9×10^{13} W/cm^2 as used in our previous works [26]. Pulse duration of all the pulses are specified as full width at half maximum (FWHM) $T_{\text{FWHM}} = 5$ opt.cyc. with respect to intensity. We choose $a(t) = [\cos(t/T_{\text{FWHM}})]^8$, similar to the Gaussian-like envelope to approximate the realistic pulses. Apart from the cos^8 envelope, a "flat-top" trapezoidal function with a linear rise and descent over a single optical cycle is also applied to simulate the long pulse. We use the flat-top envelope pulse because it is suitable to investigate the Freeman resonances.

III. NUMERICAL RESULTS

The discretization parameters used here are the same as used in our previous work in Ref. [26]. The field free ground energy value is $E_0 = -0.592$ atomic units and the internuclear distance is 2.05 atomic units. With the kinetic energy of protons excluded, the ground eigenenergy is -0.597 atomic units, three digits exact to the ground energy from quantum chemistry calculations in Ref. [30], where the internuclear distance is fixed. The internuclear distance is 1.997 atomic units, three digits exact to that from the precise computations in Ref. [31].

A. Joint energy spectra

The JES of the two dissociative protons and the electron is obtained by

$$\sigma(E_N, E_e) = \int d\phi_1 \int d\phi_2 \int d\theta_1 \sin\theta_1 \int d\theta_2 \sin\theta_2$$
$$\times P(\phi_1, \theta_1, \sqrt{4ME_N}, \phi_2, \theta_2, \sqrt{2mE_e}), \tag{17}$$

where E_N, E_e are the KERs of *two protons* and an electron, respectively. The spectrum $P(\vec{k}_1, \vec{k}_2, T)$ is from Eq. (8). $\sigma(E_N, E_e)$ is presented in Fig. 2. The blue tilt lines with formula $E_N + E_e = N\omega + E_0 - U_p$ with $U_p = \frac{A_0^2}{4m}$ specify the energy sharing of N photons for all computations. For the cos^8 envelope computations in Figs. 2(a) and 2(c), the blue dashed lines representing $E_N + E_e = N\omega + E_0 - U_p$ fall in the peak of the stripe in JES, representing the standard energy sharing signatures. For the flat-top envelope in Figs. 2(b) and 2(d), although each dashed line $E_N + E_e = N\omega + E_0 - U_p$ labels a certain tilt stripe in JES, it is not at the center of the stripes, which, however, are well described by $E_N + E_e = N\omega + E_0$. This behavior was also observed in experiments with long pulses [13] and was attributed to Freeman resonances. One also observes that the JES yield with nuclear KER $\geqslant 3$ eV are more considerable for flat-top computations, whereas the peak of JES are mainly located with nuclear KER $\leqslant 3$ eV
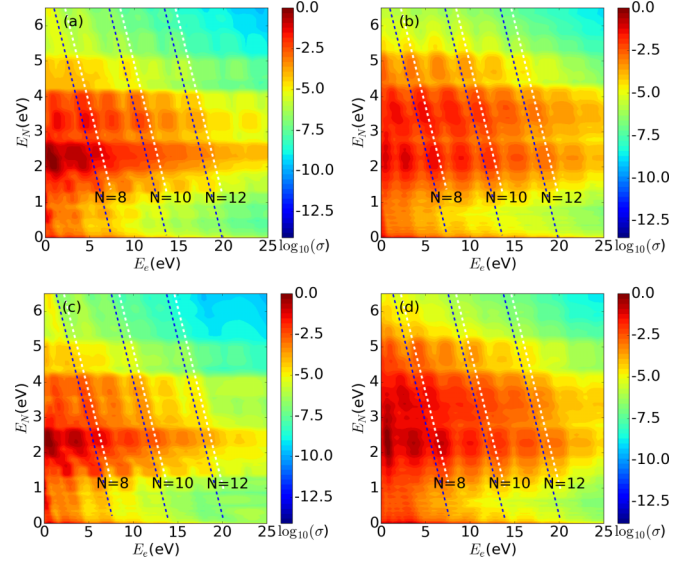

FIG. 2. Log-scale JES $\log_{10} \sigma(E_N, E_e)$ represented by total energy of two protons E_N and that of an electron E_e. Linear polarized, 400 nm, with (a) cos^8 envelope, $I = 8.3 \times 10^{13}$ W/cm^2, (b) flat-top envelope, $I = 8.3 \times 10^{13}$ W/cm^2, (c) cos^8 envelope, $I = 5.9 \times 10^{13}$ W/cm^2, and (d) flat-top envelope, $I = 5.9 \times 10^{13}$ W/cm^2 with FWHM = 5 opt.cyc. pulses are applied to the H$_2^+$ ion. The blue dashed lines represent the energy sharing between the protons and electron with formula $E_N + E_e = N\omega + E_0 - U_p$ and white ones represent $E_N + E_e = N\omega + E_0$, where ω is the photon energy.

for cos^8 computations. The Freeman resonance is expected with a flat-top envelope laser pulse with constant intensity. We will show that the "missing of U_p" in JES is from Freeman resonance and investigate the underlying mechanism in the following section.

To verify the above observation with the experimental data from references, a long (FWHM = 13 opt.cyc.), cos^8 shape laser pulse as used in Ref. [13] is applied for the calculation, where the JES is shown in Fig. 3(a). Because Freeman resonance could be expected with a long pulse [15]. In Fig. 3(a) we also find the white lines representing $E_N + E_e = N\omega + E_0$
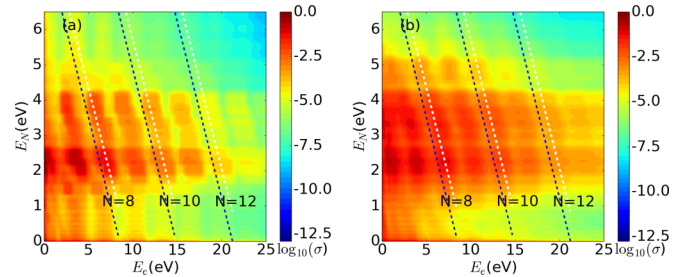

FIG. 3. Log-scale JES $\log_{10} \sigma(E_N, E_e)$ represented by total energy of two protons E_N and that of an electron E_e. Linear polarized, 390 nm at $I = 5.9 \times 10^{13}$ W/cm^2, with (a) cos^8 envelope, with FWHM = 13 opt.cyc. as used in Ref. [13], and (b) flat-top envelope FWHM = 13 opt.cyc. laser pulses are applied to the H$_2^+$ ion. The blue dashed lines represent the energy sharing between the protons and electron with formula $E_N + E_e = N\omega + E_0 - U_p$ and white ones represent $E_N + E_e = N\omega + E_0$, where ω is the photon energy.

are in the middle of the stripes in JES, whereas the blue lines representing $E_N + E_e = N\omega + E_0 - U_p$ are not, indicating a missing of U_p from Freeman resonance. Another laser pulse with flat-top envelope is also applied for a comparison with the $\cos^8$ envelope in Fig. 3(b), where the missing of U_p is also observed, consistent with the flat-top computation with 400 nm laser pulses above.

B. Wave function analysis

The resonance is usually accompanied by states mixing which contributes to populations of excited states that survive after the pulse. The probability distributions of the electron and the protons are calculated by integrating the 6D wave function on radial coordinates $r_{1/2} \in [R_0, R_1]$ and the whole angular coordinates as

$$p_N(\phi_1, \theta_1, r_1, R_0, R_1, T) = \int d\phi_2 \int \sin\theta_2 d\theta_2$$
$$\times \int_{R_0}^{R_1} r_2^2 dr_2 |\psi(\vec{r}_1, \vec{r}_2, t)|^2 \tag{18}$$

for the protons, and

$$p_e(\phi_2, \theta_2, r_2, R_0, R_1, T) = \int d\phi_1 \int \sin\theta_1 d\theta_1$$
$$\times \int_{R_0}^{R_1} r_1^2 dr_1 |\psi(\vec{r}_1, \vec{r}_2, t)|^2 \tag{19}$$

for the electron. We split the radial coordinates into the inner region and the outer region $r_{1,2} \in [R_0, R_1]$, and the yields of both regions are normalized by diving the maximum probability of the region over the flat-top and $\cos^8$ envelopes. We only focus on the wave packets after the time propagation at $t = T$ ($T \geqslant 330$ atomic units for flat-top and $T \geqslant 770$ atomic units for $\cos^8$ envelopes), because they are important for investigating the resonance.

The wave function evolution of the electron and the protons at the end of the pulse is illustrated in Fig. 4. Before analyzing the figure, we would like to point out that the values of the two regions are normalized in order to make the illustration better. The absolute values in the outer region are insignificant compared to those of the inner region; the absolute values of the outer region of the third row are much smaller than those of the first two rows. For the distribution of the electron after the pulse in the left column of Fig. 4, the yields of the inner region are similar for the flat-top and the $\cos^8$ envelopes; in the outer region, the distributions are less symmetric for the flat-top envelope, indicating a dominance for ungrade $^2\Sigma_u^+$ states. For the distribution of protons after the pulse, we scan the R_0, R_1 values and only find the existence of enhanced yields at two radial values as depicted in the right column of Fig. 4. There exist discrete peaks of yields for fat-top envelop computation, with $r_1 = 3.25, 3.7$ ($R = 2r_1 = 6.5, 7.4$) for $I = 8.3 \times 10^{13}$ W/cm^2, and $r_1 = 4.5, 4.8$ ($R = 2r_1 = 9, 9.6$) for $I = 5.9 \times 10^{13}$ W/cm^2 atomic units. These enhanced yields could serve as evidences for states mixing and Freeman resonances. However, for the $\cos^8$ envelope computation, the
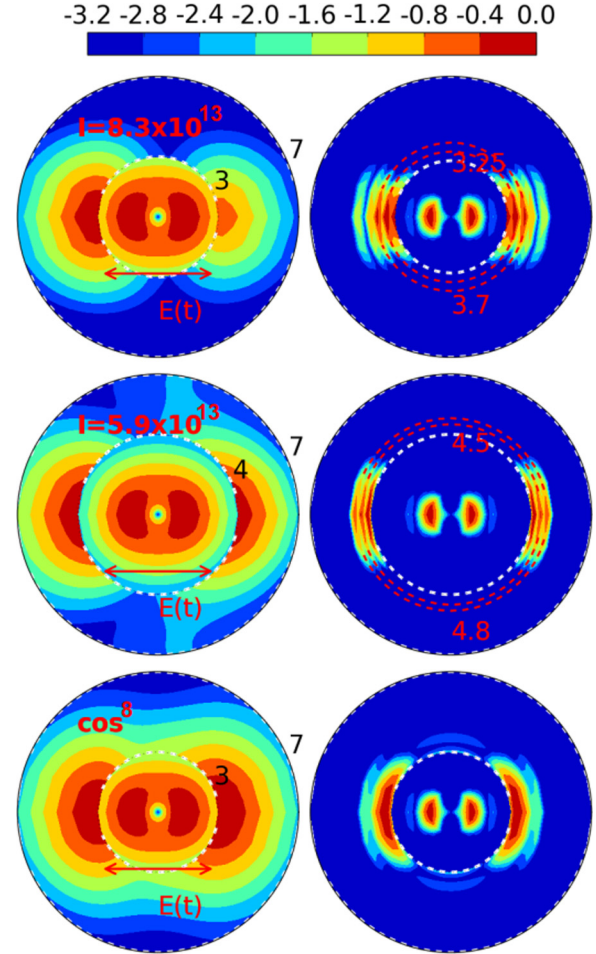

FIG. 4. The log-scale probability distribution of electron by Eq. (19) (left column) and of protons by Eq. (18) (right column) and with flat-top envelope at 8.3×10^{13} W/cm^2 (first row), 5.9×10^{13} W/cm^2 (second row), and $\cos^8$ envelope at 8.3×10^{13} W/cm^2 (third row). $[R_0, R_1]$ are [0,3] and [3,7] atomic units for the inner and outer regions of the first and third rows; $[R_0, R_1]$ are [0,4] and [4,7] atomic units for inner and outer regions of the second row. The inner and outer regions are split by the white, dashed circle along with the radial values, which are depicted in the electron figure in the left column; values of each region are both normalized by dividing the maximum number. The radial positions enhanced yields of the protons in the outside region by Eq. (18) are illustrated by the dashed red circles and ticks in the right column. The absolute value of the outer shell is several orders smaller than the inner shell. The peaks of yields of the protons near the white circle are neglected because it comes from the normalization. The polarization direction is along the horizontal axis and the direction electric field is labeled at each subfigure with an arrow above $E(t)$.

yields are contiguous and no such enhanced yields are observed.

Considering the radial position of the peaks of the enhanced yields, we find that the relative energy of the two ungrade states at the enhanced radial coordinates above are the ponderomotive energies, as is depicted by the two black vectors in Fig. 5. Thus the enhanced yields in the analysis of wave function is highly correlated with the energy transfer between these two excited states, and U_p is consumed during
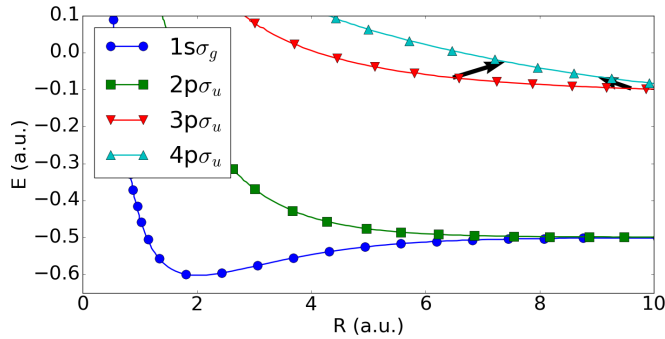
FIG. 5. The eigenstates of electrons of H_2^+ with internuclear distance R are calculated from the generalized Lambert W function [32]. The two vectors depict the energy transfer with the help of ponderomotive energy U_p. The energy transfer $4p\sigma_u(7.4) - 3p\sigma_u(6.5) = 0.0434$ atomic units with $U_p(I = 8.3 \times 10^{13} \text{ W/cm}^2) = 0.0455$ atomic units and $4p\sigma_u(9.6) - 3p\sigma_u(9) = 0.0322$ atomic units with $U_p(I = 5.9 \times 10^{13} \text{ W/cm}^2) = 0.0330$ atomic units. The small error may come from the neglect of E_N, which is not included in this figure.

this process. This contributes to the missing of U_p in JES. The internuclear distance of protons are changed during the resonance and more intermediate, excited states of protons are created. This also explains the higher yield in JES with nuclear KER $\geqslant 3$ eV for the flat-top envelope than the $\cos^8$ envelope in Fig. 2.

To sum up, from the analysis of the wave function after the end of the pulse, we find a clear signature of Freeman resonance in H_2^+ when shot by the flat-top envelope laser pulse, compared to the short, $\cos^8$ envelope laser pulse. The energy transfer between the two corresponding excited states contributes to the missing of U_p in the JES.

IV. CONCLUSION AND DISCUSSION

We computed the JES for a 400 nm pulse with flat-top envelope and $\cos^8$ envelope at 8.3×10^{13} and 5.9×10^{13} W/cm^2. In JES, the energy sharing of N photons with frequency ω by nuclear KER E_N and electronic KER E_e are well represented by $E_N + E_e = N\omega + E_0 - U_p$ for $\cos^8$ pulses, but satisfy $E_N + E_e = N\omega + E_0$ for the flat-top envelope. The difference comes from the ungerade excited states with energy difference U_p. We propose that this is a universal effect for an arbitrary intensity as the eigenenergies of H_2^+ are contiguous with the bound length R. At higher intensities there may also exist other resonance states with energy difference $N\omega + U_p$, which requires further investigation.

[1] P. H. Bucksbaum, A. Zavriyev, H. G. Muller, and D. W. Schumacher, Phys. Rev. Lett. **64**, 1883 (1990).

[2] T. Zuo and A. D. Bandrauk, Phys. Rev. A **52**, R2511(R) (1995).

[3] G. Yao and S.-I Chu, Phys. Rev. A **48**, 485 (1993).

[4] A. Giusti-Suzor, F. H. Mies, L. F. DiMauro, E. Charron, and B. Yang, J. Phys. B At. Mol. Opt. Phys. **28**, 309 (1995).

[5] G. Jolicard and O. Atabek, Phys. Rev. A **46**, 5845 (1992).

[6] T. Zuo, S. Chelkowski, and A. D. Bandrauk, Phys. Rev. A **48**, 3837 (1993).

[7] J. H. Posthumus, Reports Prog. Phys. **67**, 623 (2004).

[8] A. Giusti-Suzor, X. He, O. Atabek, and F. H. Mies, Phys. Rev. Lett. **64**, 515 (1990).

[9] L. Yue and L. B. Madsen, Phys. Rev. A **88**, 063420 (2013).

[10] L. Yue and L. B. Madsen, Phys. Rev. A **90**, 063408 (2014).

[11] M. Odenweller, N. Takemoto, A. Vredenborg, K. Cole, K. Pahl, J. Titze, L. P. H. Schmidt, T. Jahnke, R. Dörner, and A. Becker, Phys. Rev. Lett. **107**, 143004 (2011).

[12] M. Odenweller, J. Lower, K. Pahl, M. Schütt, J. Wu, K. Cole, A. Vredenborg, L. P. Schmidt, N. Neumann, J. Titze, T. Jahnke, M. Meckel, M. Kunitski, T. Havermeier, S. Voss, M. Schöffler, H. Sann, J. Voigtsberger, H. Schmidt-Böcking, and R. Dörner, Phys. Rev. A At. Mol. Opt. Phys. **89**, 013424 (2014).

[13] J. Wu, M. Kunitski, M. Pitzer, F. Trinter, L. P. H. Schmidt, T. Jahnke, M. Magrakvelidze, C. B. Madsen, L. B. Madsen, U. Thumm, and R. Dörner, Phys. Rev. Lett. **111**, 023002 (2013).

[14] X. Gong, P. He, Q. Song, Q. Ji, K. Lin, W. Zhang, P. Lu, H. Pan, J. Ding, H. Zeng, F. He, and J. Wu, Optica **3**, 643 (2016).

[15] R. R. Freeman, P. H. Bucksbaum, H. Milchberg, S. Darack, D. Schumacher, and M. E. Geusic, Phys. Rev. Lett. **59**, 1092 (1987).

[16] L. Tao and A. Scrinzi, New J. Phys. **14**, 013021 (2012).

[17] A. Zielinski, V. P. Majety, and A. Scrinzi, Phys. Rev. A **93**, 023406 (2016).

[18] J. Zhu and A. Scrinzi, Phys. Rev. A **101**, 063407 (2020).

[19] G. L. V. Steeg, K. Bartschat, and I. Bray, J. Phys. B At. Mol. Opt. Phys. **36**, 3325 (2003).

[20] W. Qu, Z. Chen, Z. Xu, and C. H. Keitel, Phys. Rev. A **65**, 013402 (2001).

[21] R. E. F. Silva, F. Catoire, P. Rivière, H. Bachau, and F. Martín, Phys. Rev. Lett. **110**, 113001 (2013).

[22] C. B. Madsen, F. Anis, L. B. Madsen, and B. D. Esry, Phys. Rev. Lett. **109**, 163003 (2012).

[23] N. Takemoto and A. Becker, Phys. Rev. Lett. **105**, 203004 (2010).

[24] B. Feuerstein and U. Thumm, Phys. Rev. A At. Mol. Opt. Phys. **67**, 043405 (2003).

[25] K. C. Kulander, F. H. Mies, and K. J. Schafer, Phys. Rev. A **53**, 2562 (1996).

[26] J. Zhu, Phys. Rev. A **102**, 053109 (2020).

[27] J. R. Hiskes, Phys. Rev. **122**, 1207 (1961).

[28] A. Scrinzi, New J. Phys. **14**, 085008 (2012).

[29] A. Scrinzi, Phys. Rev. A **81**, 053845 (2010).

[30] D. Bressanini, M. Mella, and G. Morosi, Chem. Phys. Lett. **272**, 370 (1997).

[31] L. J. Schaad and W. V. Hicks, J. Chem. Phys. **53**, 851 (1970).

[32] T. C. Scott, M. Aubert-Frécon, and J. Grotendorst, Chem. Phys. **324**, 323 (2006).